Progress In Electromagnetics Research B, Vol. 70, 1–12, 2016

Diamagneto-Dielectric Anisotropic Wide Angle Impedance Matching Layers for Active Phased Arrays

Fabrizio Silvestri[1, 2, *], Lorenzo Cifola[3], and Giampiero Gerini[1, 2]

Abstract—In this paper, we present the full process of designing anisotropic metamaterial (MM) wide angle impedance matching (WAIM) layers. These layers are used to reduce the scan losses that occur in active phased arrays for large scanning angles. Numerical results are provided to show the improvement in performances that such layers can ensure. The proposed anisotropic MM-WAIM layers achieve an improvement of about 1 dB of more radiated power at $\theta = 70°$ from broadside, in a 13% of fractional bandwidth on the azimuthal plane $\phi = 90°$. Weaker improvements are obtained in the other azimuthal planes, however keeping the active reflection coefficient below -9 dB for all azimuthal planes up to $\theta = 60°$ and up to $\theta = 70°$ off-axis for planes $\phi = 45°, 90°$ in the whole operational band.

1. INTRODUCTION

Active phased arrays, which are already widely used for radar systems, are more and more often used also for satellite communication applications on board of mobile platforms, thanks to their extreme flexibility in steering and shaping electronically their beam. In most of the cases, active phased arrays with large angular coverage are required. Such performances are important not only for the operational scanning characteristics of phased arrays, but also for compensating any misalignment due to the movements of the mounting platforms. The scanning characteristics of phased arrays are however limited and different solutions to mitigate this issue have been investigated already several decades ago [1, 2]. The scanning limitations are caused by two mechanisms: reduction of the antenna effective area and the variation of the mutual coupling among the different elements of the array when scanning. The variation of mutual coupling can be understood referring to the concept of the active impedance or scan impedance [3]. Assuming an (infinite) periodic lattice of equal antennas, the active impedance is defined as the input impedance of one single element, when all the elements are radiating. The variation of the coupling between the array elements under different scanning conditions determines also a variation of the active impedance. This clearly results in a mismatch between the antenna and the electronic modules, for large scanning angles. Two solutions have been conceived, till now, in order to increase the impedance matching: one relies on the insertion of additional dielectric layers above the phased arrays [1], the other one is based on the use of inter-elements connecting circuits [2]. A solution based on dielectric layers, placed above the radiating elements, does not require a complex design and, more important, can be applied without modifying an existing phased array design. In this perspective, the strategy based on additional layers is preferable and mostly used.

The typical design parameters of wide angle impedance matching (WAIM) layers are: the number of layers, their thickness, the distances between each layer and the antenna and their dielectric

Received 28 June 2016, Accepted 14 September 2016, Scheduled 22 September 2016

* Corresponding author: Fabrizio Silvestri (fabrizio.silvestri@tno.nl).

[1] Optics Department, Netherlands Organization for Applied Scientific Research, TNO, Stieltjesweg 1,2628CK Delft, The Netherlands. [2] Electromagnetics Group, Eindhoven Technology University, TU/e, Den Dolech 2, 5600MB Eindhoven, The Netherlands. [3] was with the Netherlands Organization for Applied Scientific Research, TNO and he is now with Thales Nederland B.V., Advanced Development Delft, Delftechpark 24, 2628 XH Delft, The Netherlands.

characteristics. These parameters can be determined with an optimization process. Among all the design parameters, the dielectric permittivity and magnetic permeability represent the main limitations, since only a limited number of materials, with the required electrical and mechanical characteristics, are commercially available. In any case these materials offer only a limited discrete range of values of electrical parameters (permittivity and permeability). For this reason, new concepts based on artificially engineered materials, usually called metamaterials (MM), must be explored, exploiting their capability to synthesize electrical characteristics not available in nature.

MMs are usually composed of infinite periodic lattices of dielectric or metal scatterers embedded in a host dielectric substrate. The scatterers have sub-wavelength dimensions in the order of $\lambda/20$–$\lambda/10$. This allows a homogenization process, in which the combination of scatterers and substrate can be electromagnetically described as an effective homogeneous material. Playing with the geometrical/electrical parameters of the scatterers, it is possible to achieve effective dielectric and magnetic parameters with isotropic or anisotropic characteristics [4–6].

Due to their birefringent behaviour, homogeneous anistropic layers can be exploited to match the angular dependence of the active impedance of phased arrays, giving further degrees of freedom in the WAIM layers design [7–9]. The definition of proper constraints and cost-function, is essential for the design of anisotropic WAIM layers. Previous works on the topic have dealt either with only dielectric anisotropic material models [8, 9] or, although presenting ideal cases of dielectric-magnetic MM, with final MM structures that exhibit only a dielectric behaviour [7]. The aim of this paper is to present a design approach for MM-WAIM structures based on requirements in terms of angular coverage and bandwidth, highlighting the issues and the limits in the realization of MMs. In order to reach sufficient performances for realistic radar applications, we present a structure characterized by a diamagneto-dielectric behaviour. The paper is structured as follows: in Section 2 the theoretical background, the modeling tools and the optimization procedure of the design strategy are presented. In Section 3, the results obtained by using this design strategy are presented and discussed.

2. DESIGN STRATEGY

The design of anisotropic WAIM layers, optimized in the presence of the array antenna, is performed by coupling a full-wave model of the active phased array under consideration, with an analytical model describing the WAIM layers [10]. The active phased array under study is an infinite periodic array of equal radiating elements excited with linear progressive phases. The radiated fields of an infinite periodic array can be expanded with a set of discrete Floquet modes and the propagation of each mode can be modeled with a simple equivalent transmission line model. In this way, the interaction between the fields radiated by the array and any homogeneous anisotropic layer, placed above the antenna, can be modeled with a set of uncoupled transmission lines [11], as shown in Figure 1.

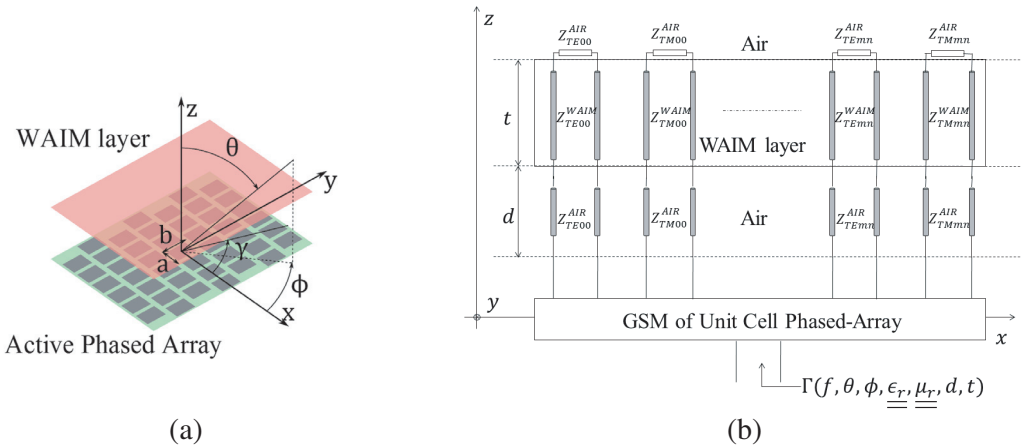

Figure 1. (a) Geometry of the problem, (b) equivalent model composed of the GSM for the active phased array and transmission lines for the WAIM layer.

Actually, each transmission line consists of a cascade of lines with different properties, according to the different media present above the array.

The electromagnetic field excited by the array antenna can be found with analytical models, when canonical structures are involved, e.g., rectangular and circular apertures, printed dipoles or slots [7, 8, 12–14] or resorting to full-wave simulations, enabling the analysis of more complex structures. For this work, we have used the finite-element (FEM) solver of Ansys HFSS ® [15].

Once the generalized scattering matrix (GSM) of the array is computed, its modal ports can be connected to the corresponding modal ports of the transmission lines representing the overlaying structure (air-gap and WAIM). At this point, it is possible to compute the active input impedance or the active reflection coefficient at the input port of each radiating element. The closer the WAIM layer is to the phased array, the higher its effect on the impedance matching is. In such a case, the evanescent Floquet modes, excited at the antenna aperture, are still accessible and they can interact with the discontinuity created by the WAIM layer, modifying the mutual coupling between elements and therefore the active impedance at each radiating element. Assuming a material characterized by magnetic and dielectric diagonal tensors

$$\underline{\underline{\epsilon_r}} = \epsilon_x \hat{\mathbf{x}}\hat{\mathbf{x}} + \epsilon_y \hat{\mathbf{y}}\hat{\mathbf{y}} + \epsilon_z \hat{\mathbf{z}}\hat{\mathbf{z}}, \quad \underline{\underline{\mu_r}} = \mu_x \hat{\mathbf{x}}\hat{\mathbf{x}} + \mu_y \hat{\mathbf{y}}\hat{\mathbf{y}} + \mu_z \hat{\mathbf{z}}\hat{\mathbf{z}} \tag{1}$$

where x-y are the directions of the transverse plane of the array, and z is the direction of propagation, the transverse impedance and wave-numbers can be computed according to the Floquet theory [17]:

$$Z_{TE} = \frac{\omega \mu_0 \mu_x}{k_{z,TE}}, \quad k_{z,TE}^{mn} = \sqrt{k_0^2 \mu_x \epsilon_y - k_{t,mn}^2 \frac{\mu_x}{\mu_z}} \tag{2}$$

$$Z_{TM} = \frac{k_{z,TM}}{\omega \epsilon_0 \epsilon_x}, \quad k_{z,TM}^{mn} = \sqrt{k_0^2 \mu_y \epsilon_x - k_{t,mn}^2 \frac{\epsilon_x}{\epsilon_z}} \tag{3}$$

$$k_{t,mn}^2 = k_{x,mn}^2 + k_{y,mn}^2 \tag{4}$$

$$k_{x,mn} = k_0 \sin\theta \cos\phi + \frac{2m\pi}{a} \tag{5}$$

$$k_{y,mn} = k_0 \sin\theta \sin\phi - \frac{2m\pi}{a \tan\gamma} + \frac{2n\pi}{b} \tag{6}$$

where k_0 is the wave-number in vacuum; a, b are the lattice array dimensions; γ is the triangular grid angle, as shown in Figure 1. In this contribution, we will consider only materials characterized by diagonal tensors with $\mu_x = \mu_y$ and $\epsilon_x = \epsilon_y$. For a linear polarized array, with the source aligned in the x direction, the active realized gain for the copolar components, according to the Ludwig third definition [16], is expressed as

$$G_{co}(\theta, \phi) = \frac{4\pi A \cos\theta}{\lambda^2} \left| S_{21}^{TM}(\theta, \phi) \cos\phi + S_{21}^{TE}(\theta, \phi) \sin\phi \right|^2 \tag{7}$$

where S_{21}^{TM} and S_{21}^{TE} are the transmission coefficients for the two specular fundamental Floquet modes, and A is the area of the array unit cell [17]. It is clear that, in order to match the active impedance over a large angular range, at least for the two cardinal planes, $\phi = 0°, 90°$, we need to act on both the polarizations. The dielectric and magnetic tensors entries, the layer thickness t and the distance d from the antenna plane are the design parameters of the anisotropic WAIM layer. The optimal values of the parameters are determined through a numerical optimization process. Better results can be obtained with a cost function with adaptive weights, instead of using cost functions based on an average behavior of the active reflection coefficient, over all the operational conditions [7–9]. The cost function used is defined as follows:

$$\sum_f \sum_\phi \sum_\theta \alpha(f, \theta, \phi) \left| \Gamma\left(\underline{\underline{\epsilon}}, \underline{\underline{\mu}}, t, d; f, \theta, \phi\right) \right|^2. \tag{8}$$

The adaptive weights $\alpha(f, \theta, \phi)$ are different for each operative situation and defined following this strategy [18]:

$$\alpha(f, \theta, \phi) = \begin{cases} 0 & \text{if } |\Gamma|_{\text{dB}} < \text{thresh}|_{\text{dB}} \\ |\Gamma|_{\text{dB}} - \text{thresh}|_{\text{dB}} & \text{if } |\Gamma|_{\text{dB}} \geq \text{thresh}|_{\text{dB}}. \end{cases} \tag{9}$$

For this work, we have used the MATLAB ® [19] constrained nonlinear optimization solver. Constraints can be used to limit the range of the design parameters.

Once the optimal set of electrical and geometrical parameters for the WAIM layer has been found, it must be translated into a physical design. For this purpose, MM unit cells are analyzed with full-wave simulations and from these through a homegenization procedure, the effective parameters of the structures can be extracted. The type of parameters extracted depends on the homogenization equivalence principle imposed [20]. In the case of WAIM layer design, the external equivalence (the MM scattered transverse components must be equal to the transverse components scattered by a homogeneous equivalent layer) is sufficient, because the interaction between the array and the WAIM is modeled through their GSMs. This type of equivalence is the starting point for retrieval algorithms based on reflection and transmission properties of MM slabs [21, 22]. MMs with pronounced spatial dispersion effects, might not be employed in the current WAIM layer design, unless different hypothesis on the model of the anisotropic WAIM layer are made, i.e., exploitation of the permittivity and permeability tensors dependency with angle of incidence. In the following section, we will show how the design strategy for the anisotropic WAIM layers and the MM homogenization algorithms can be used to design realizable and effective MM-WAIM layers.

3. RESULTS

In this section, we discuss the results of the design methodology, exposed in the previous section, applied to an active phased array. The array has a fractional bandwidth of 13% in the microwave band (active reflection coefficient $\Gamma \leq -10\,\mathrm{dB}$). The array consists of capacitively fed stacked patch elements working in linear polarization. The exact geometry of the array cannot be disclosed and in any case it is not relevant for this paper, since the array is, in fact, used as a "black-box" and its geometry is not modified during the WAIM design. It is worth mentioning that, being a realistic phased array, the scan losses exhibited by the array are only due to the geometric effective area reduction and impedance mismatching. Any other effect, such as surface waves or grating lobes, is not present. The first step of the design procedure consists of building a database of GSMs, modeling the phased array for different frequencies and scanning directions. The number of modes, used in the simulations, has been chosen following an analysis of the excited modes at the free-space port. It has been found that 20 Floquet modes are enough to represent the field at the output port of the unit cell, under all the different scanning conditions. The optimization has been performed over three planes, E-plane, $\phi = 0^\circ$, D-plane, $\phi = 45^\circ$ and H-plane, $\phi = 90^\circ$, using 5 frequency samples. For sake of brevity, we will show the results only for the lowest, uppest and central frequencies; for the intermediate ones, similar behaviors have been found. The threshold level used in the adaptive scheme is $-10\,\mathrm{dB}$. For the different WAIM layers designs, the variation of the active realized copolar gain, $G_{co}(\phi, \theta)$, with the scanning angles, at different frequencies, is presented. Analyzing this parameter, it is possible to check the effect of surface waves, which might be present in the WAIM structure, on the phased array radiation characteristics. Furthermore, this also allows to evaluate how the WAIM affects the polarization characteristics of the array.

3.1. Magneto-Dielectric Anisotropic WAIM

In the first step, we have applied our design strategy to a situation in which only loose constraints on the design parameters are imposed. This could lead to an optimal solution, in terms of performances, but difficult to be realized using MMs. Such a solution is used as baseline for comparison with the other designs.

The electrical parameters are limited only within intervals that do not include extreme conditions, such as negative or near-zero values, to ensure broadband and wide-angle performances. The values of the constrain intervals and the optimal set of parameters are reported in Table 1. The performances of an anisotropic WAIM layer characterized by this optimal set of parameters are shown in Figure 2. In the graphs, the power difference between the radiated fields of a phased array with the anisotropic layer and the radiated fields of a phased array without the WAIM is plotted. From the plots it can be noted that, in average over all the three planes, there is a high improvement in performances for large angles. At the

Table 1. Optimal values of the magneto-dielectric anisotropic WAIM layer found solving the constrained optimization problem.

Design Parameter	Constrained Interval	Optimal Value
$\epsilon_x = \epsilon_y$	$[0.5, 7]$	0.86
ϵ_z	$[0.5, 7]$	0.5
$\mu_x = \mu_y$	$[0.5, 6]$	1.37
μ_z	$[0.5, 6]$	5.3
d	$[0.068, 0.43]\lambda_0$	$0.068\lambda_0$
t	$[0.052, 0.31]\lambda_0$	$0.089\lambda_0$

highest frequency, the maximum gain is achieved on the E-plane, at $\theta = 70°$, with an improvement of almost 2.75 dB, which corresponds to 88% more power radiated with the anisotropic WAIM, compared with the phased array without any matching layer. For angles around $\theta = 40°$–$50°$, the performances are slightly worse than the ones of the array alone (as worst case: -0.1 dB/-2% and -0.13 dB/-3% at $\theta = 40°, 50°$ for the D-plane at the central frequency). The small decrease in this angular range is mainly due to the particular scanning properties of the phased array under examination, which is well matched around $\theta = 40°$ ($\Gamma \in [-15, -20]$ dB). Nevertheless, the active reflection coefficient is kept below the required threshold by the adaptive optimization strategy.

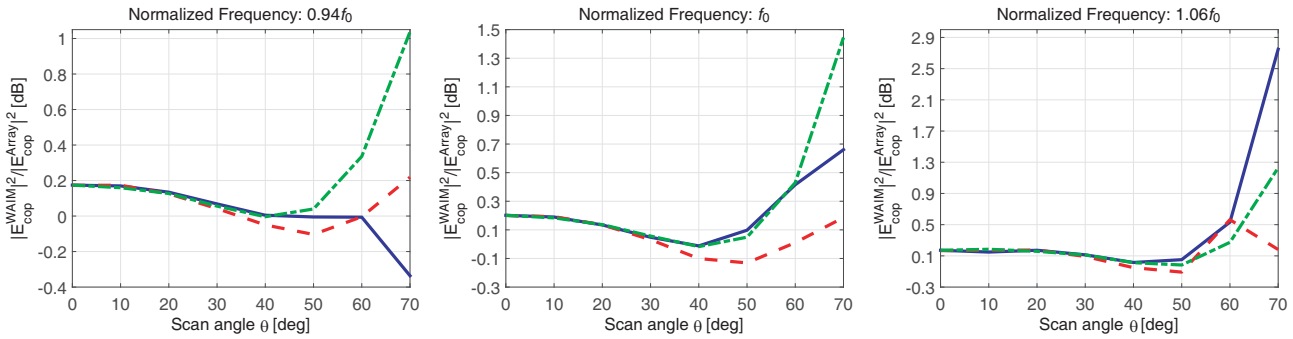

Figure 2. Ratio between the copolar gain components of the phased-array with and without the optimized anisotropic magneto-dielectric WAIM layer; the ratio is presented as function of the scan angle off broadside θ, for different azimuthal planes and frequencies (solid blue line: E-plane; dashed red line: D-plane; dot-dashed green line: H-plane).

Despite the constraints imposed in the optimization, the optimal parameters reported in Table 1 cannot be easily realized using MMs, considering the requirements imposed by the particular EM scenario, i.e., frequency bandwidth, range of angular directions of the incoming beams, polarization characteristics. First of all a magnetic response is required to obtain a good matching for all planes. In fact, by examining Equations (2), (7), it is clear that, in order to affect both polarizations, the WAIM layer must be characterized by both an anisotropic magnetic and dielectric behavior. Typical MM structures employed to achieve a magnetic response are split ring resonators (SRRs) [5, 23]. However, these are characterized by extreme narrowband and high angular dispersive behavior, in contrast with the application requirements (bandwidth of 13%, angular directions up to 70°, both TE and TM polarization excitations). For this reason MM-WAIM layers without a magnetic behaviour have been studied and they are presented in the next subsections.

3.2. Dielectric-Only Anisotropic WAIM Layers

Artificial dielectrics have been studied since the pioneering work on multilayer structures [24]. The main advantage of artificial dielectrics is that anisotropic dielectrics can be built by simply stacking layers of different homogeneous materials with sub-wavelength thickness. An artificial anisotropic material can be realized stacking along the z direction (normal to the material surface) two different materials, characterized by two different permittivities (ϵ_1, ϵ_2) and thicknesses (t_1, t_2), to form a unit cell that is repeated in one dimension. For this type of MM, the equivalent dielectric parameters are [24]:

$$\epsilon_x = \epsilon_y = \epsilon_1 p + \epsilon_2 (1-p) \tag{10}$$

$$\epsilon_z = [\epsilon_1^{-1} p + \epsilon_2^{-1} (1-p)]^{-1} \tag{11}$$

where $p = t_1/(t_1 + t_2)$ is the filling ratio. The new constraints, used to optimize the design parameters of the WAIM layer, are reported in Table 2, together with the corresponding optimal values.

Table 2. Optimal values of the dielectric-only anisotropic WAIM layer found solving the constrained optimization problem.

Design Parameter	Constrained Interval	Optimal Value
$\epsilon_x = \epsilon_y$	$[0.5, 10]$	1.15
ϵ_z	$[0.5, 10]$	0.87
$\mu_x = \mu_y = \mu_z$	1	1
d	$[0.068, 0.43]\lambda_0$	$0.097\lambda_0$
t	$[0.052, 0.31]\lambda 0$	$0.248\lambda_0$

An anisotropic WAIM layer, with the parameters of Table 2, improves the angular performances at large angles from broadside. However, the performances are slightly worse than the ones of the magneto-dielectric WAIM, shown in Figure 2. Furthermore realizing a MM with dielectric tensor entries smaller than one ($\epsilon_z = 0.87$) in the microwave band is not easy. According to (10), (11), the range of values that can be achieved, by just stacking dielectric layers, is limited by the available materials. In the microwave regime, there are no homogeneous materials characterized by low losses and real permittivity less than one. Nevertheless, considering that the optimal values $\epsilon_x, \epsilon_y, \epsilon_z$ are all close to unity, it is interesting to evaluate the performances of a stacked-layer dielectric-only MM-WAIM, realized with low losses available materials. For example, using commercially available layers of Duroid ® ($\epsilon_r = 2.2$) and foam ($\epsilon_r = 1.06$), with a filling ratio $p = 0.079$, it is possible to obtain an anisotropic dielectric characterized by $\epsilon_x = \epsilon_y = 1.15, \epsilon_z = 1.07$. Since these dielectric permittivities are different from the optimal ones, a new optimization has been run to find the optimal distance and thickness of this substrate from the phased array. The whole set of parameters of this layer are reported in Table 3, the perfomances of such anisotropic WAIM layer are reported in Figure 3. Figure 3 reports also the performances of a homogeneous layer of Duroid® ($\epsilon_r = 2.2$) with optimized thickness ($t = 0.052\lambda_0$) and distance ($d = 0.139\lambda_0$). This layer has been chosen as the one with best performances among the different material commercially available. The comparison shows that both WAIM layers, the anisotropic and isotropic ones, cannot increase the scanning performances of the phased array on the E-plane. It must be noted that the anisotropic MM-WAIM layer, realized stacking homogeneous dielectric layers, has better performances on the D/H-planes, at large angles from broadside, than the isotropic version.

3.3. Multilayer Diamagneto-Dielectric Anisotropic WAIM

As discussed before, MMs with magnetic response are, in principle, not suitable for WAIM applications, due to their limited bandwidth. However, this limitation does not apply to MMs with diamagnetic response. This kind of MMs can be realized with sub-wavelength conductive loops printed on dielectric substrates. The magnetic dipole, induced by the incident magnetic field component normal to the loop, radiates a field that is opposite to the incident field [23, 25]. The macroscopic effect is a decrease of

Table 3. Optimal values of the dielectric-only anisotropic WAIM layer, constraining $\epsilon_x = \epsilon_y = 1.15, \epsilon_z = 1.07, \mu_x = \mu_y = \mu_z = 1$.

Design Parameter	Optimal Value
$\epsilon_x = \epsilon_y$	1.15
ϵ_z	1.07
$\mu_x = \mu_y = \mu_z$	1
d	$0.126\lambda_0$
t	$0.209\lambda_0$

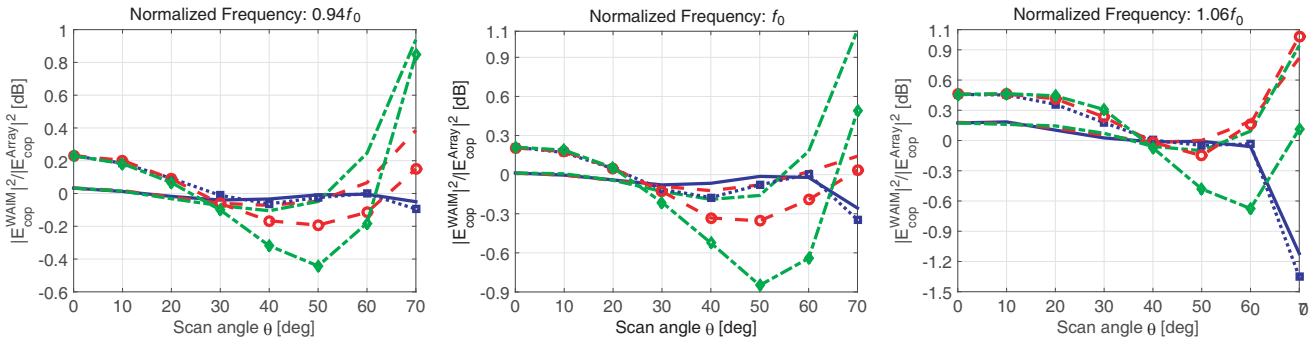

Figure 3. Ratio between the copolar gain components of the phased-array with and without the dielectric-only anisotropic WAIM layer whose parameters are reported in Table 3; the ratio is presented as function of the scan angle off broadside θ, for different azimuthal planes and frequencies. Lines without markers refer to dielectric-only anisotropic WAIM layer presented in Table 3 for the three different planes (solid blue line: E-plane; dashed red line: D-plane; dot-dashed green line: H-plane) while the lines with markers refer to a homogeneous isotropic dielectric layer, optimized in thickness and distance, with dielectric permittivity $\epsilon_r = 2.2$ for different planes (dotted blue line with squares: E-plane; dashed red line with circles: D-plane; dot-dashed green line with diamonds: H-plane).

the equivalent magnetic permeability of the MM to values lower than the magnetic permeability of the host medium. The field scattered by a sub-wavelength loop can be described, in first approximation, by two equivalent dipoles, one magnetic and the other electric. The latter produces an increase of the equivalent dielectric permittivity of the material in the directions parallel to the surface of the ring [23], whereas the magnetic dipole is responsible for the decrease of magnetic permeability. There are two main advantages in using a diamagnetic-dielectric layer in a WAIM stack. First, having ratios μ_x/μ_z, ϵ_x/ϵ_z different from one, this material affects both TE and TM polarization. Second, the magnetic polarization of the conductive loop has a quite flat frequency dispersive behavior, so the equivalent magnetic permeability of this MM is characterized by a uniform behavior in frequency [25].

First a conductive loop has been designed, with its normal aligned along the z-direction, to obtain the maximum degree of anisotropy, μ_x/μ_z. In this way, we can achieve the maximum effect on the TE polarization. The values $\epsilon_x = \epsilon_y$ are, in principle, not the optimal ones to have a single layer anisotropic WAIM. However, other dielectric-only anisotropic layers can be added to increase the number of degrees of freedom, in order to achieve a good matching over all frequencies and angular ranges. In order to optimize the dielectric-only layers, the parameters of the diamagneto-dielectric layer have been considered fixed in the optimization. An artistic impression of the whole final structure is reported in Figure 4. The constraints used in the optimization and the optimal parameters are reported in Table 4.

Full-wave simulations of the diamagneto-dielectric slab have been performed to find a geometry that provides the maximum degree of anisotropy (μ_x/μ_z). The slab consists of a Duroid® substrate,

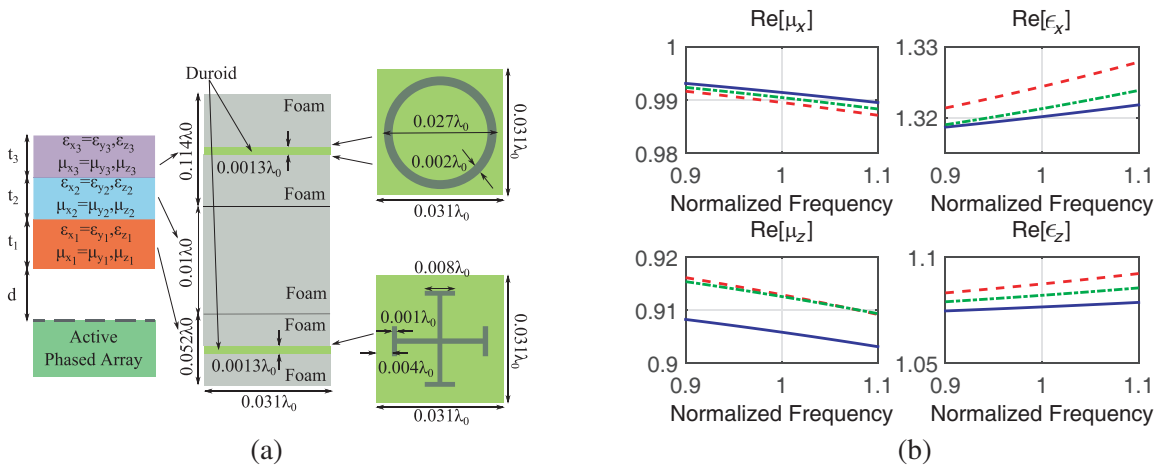

Figure 4. (a) Artistic impression of the three layers diamagneto-dielectric WAIM and its realization. Phased array and the three layers WAIM (left), x-z cross section of the three layers stack (center), x-y plane of the two MMs inclusions (right). The conductive rings are printed on both side of the substrate, whereas the conductive Jerusalem crosses only on the upper side. (b) Retrieved equivalent parameters for the diamagneto-dielectric layer, third layer from the bottom. The different curves represent the parameters behavior towards frequencies for different couple of incident plane waves: blue solid line $\theta = 40°$–$70°$, red dashed line $\theta = 10°$–$40°$, green dot-dashed line $\theta = 30°$–$50°$.

sandwiched between two symmetric foam layers, and of two conductive rings (assumed as perfect electric conductors, PECs) printed on both sides of the substrate. From the GSM of this cell alone, we can extract the equivalent parameters, reported in Figure 4. For this MM layer, spatial dispersion effects are visible, but they do not introduce extreme variations in the parameters, and therefore the effective dielectric and magnetic parameters can be considered almost uniform for all angles of incidence and over the whole band. The second step consists in optimizing the two layers below the diamagneto-dielectric layer. The first layer, just above the phased array, can be implemented with a conductive Jerusalem cross

Table 4. Optimal values of the multilayer diamagneto-dielectric WAIM for the first phased array under test.

Design Parameter	Constrained Interval	Optimal Value
$\epsilon_{x1} = \epsilon_{y1}$	$[1, 10]$	1.36
ϵ_{z1}	$[1, 10]$	1
$\mu_{x1} = \mu_{y1} = \mu_{z1}$	1	1
t_1	$[0.052, 0.31]\lambda_0$	$0.052\lambda_0$
$\epsilon_{x2} = \epsilon_{y2}$	$[1, 10]$	1.02
ϵ_{z2}	$[1, 10]$	1
$\mu_{x2} = \mu_{y2} = \mu_{z2}$	1	1
t_2	$[0.052, 0.31]\lambda_0$	$0.101\lambda_0$
$\epsilon_{x3} = \epsilon_{y3}$	1.33	1.33
ϵ_{z3}	$[1, 10]$	1.08
$\mu_{x3} = \mu_{y3} =$	1	1
$\mu_{z3} =$	0.91	0.91
t_3	$0.114\lambda_0$	$0.114\lambda_0$
d	$[0.068, 0.43]\lambda_0$	$0.114\lambda_0$

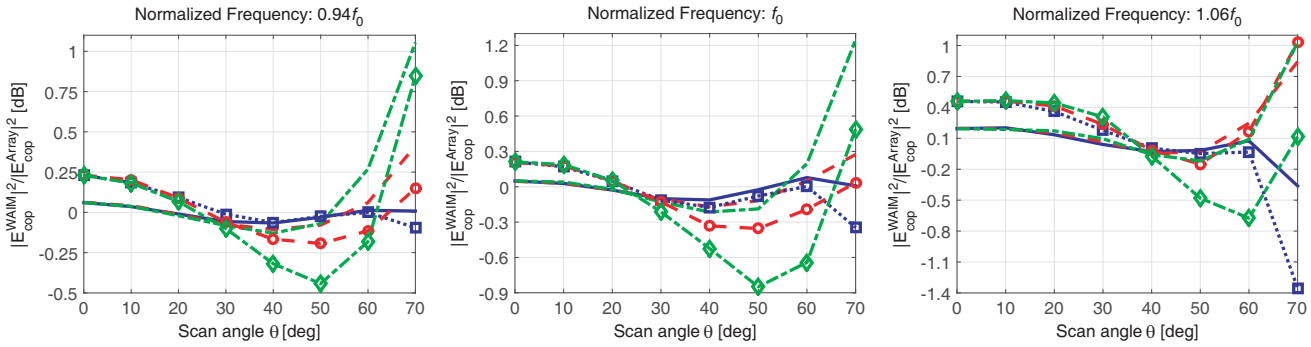

Figure 5. Ratio between the copolar gain components of the phased-array with and without the multilayer anisotropic diamagneto-dielectric WAIM whose parameters are reported in Table 4; the ratio is presented as function of the scan angle off broadside θ, for different azimuthal planes and frequencies. Lines without markers refer to the multilayer diamagneto-dielectric WAIM presented in Table 4 for the three different planes (solid blue line: E-plane; dashed red line: D-plane; dot-dashed green line: H-plane) while the line with markers refer to a homogeneous isotropic dielectric layer, optimized in thickness and distance, with dielectric permittivity $\epsilon_r = 2.2$ for different planes (dotted blue line with squares: E-plane; dashed red line with circles: D-plane; dot-dashed green line with diamonds: H-plane).

like structure. The second layer, instead, can be easily realized with a homogeneous layer of foam. The performances of this multilayer diamagneto-dielectric WAIM are reported in Figure 5, together with the performances of the homogeneous isotropic dielectric WAIM layer, already described in Subsection 3.2. For all frequencies and ϕ-planes, the multilayer WAIM provide a substantial improvement, compared to a standard technology. Although it has worse performances at directions close to broadside, at large scanning angles, the multilayer ensures always more radiated power than the homogeneous WAIM layer at large angles ($\theta \geq 40°$). Moreover comparing the results of these two configurations, Figure 3 and Figure 5, it is evident that the multilayer WAIM allows to increase the angular ranges up to 70° from broadside, also on the E-plane, where, instead, the dielectric-only WAIM layer, does not result in any improvement. Full-wave simulations of the multilayer WAIM on top of the phased array have been performed to validate the design. The phased array GSM and the three layers GSMs have been computed separately, then connected together to give the overall scattering characteristics. The GSM of the multilayer WAIM is characterized by a diagonal-block structure, as reported in Figure 6. The GSM coefficients are reported only for a particular set of frequency and scanning directions, but similar behavior have been found in other operational conditions. Therefore the coupling between different Floquet modes of the phased array is negligible, confirming the hypothesis under which the MM-WAIM layers have been homogenized and modeled as uncoupled transmission lines.

The improvement in the active realized gain, computed through full-wave simulations, compared to what obtained with the semi-analytical design procedure, is reported in Figure 7. The comparison shows almost perfect agreement between full-wave results and semi-analytical results on the D-plane and H-plane, but some differences on the E-plane, especially for large scanning angles. The full-wave numerical results show that the multilayer diamagneto-dielectric MM-WAIM modifies the scanning performances of the phased array under test in a similar fashion to an optimized homogeneous layer for the E-plane, instead slightly better improvements can be seen for the D-plane (7% of more radiated power at $\theta = 70°$ for $0.94f_0$, 3% at $\theta = 70°$ for f_0, 19% for $1.06f_0$), whereas a significant increasing of the gain, especially for large scanning angles, characterizes the behavior of the multilayer engineered WAIM on the H-plane (24% of power gain at $\theta = 70°$ at the extremes of the band and 30% at the central frequency). Although not shown here, the active reflection coefficient with the multilayer MM-WAIM is kept below -9.8 dB up to 70° off broadside direction on planes $\phi = 45°, 90°$ on the whole band. On the E-plane, as the plot of the gain suggests, the active reflection coefficient does not match the threshold requirements, nevertheless its behavior is not deteriorated by the insertion of the MM-WAIM, apart in the condition $\theta = 70°$ at $1.06f_0$.

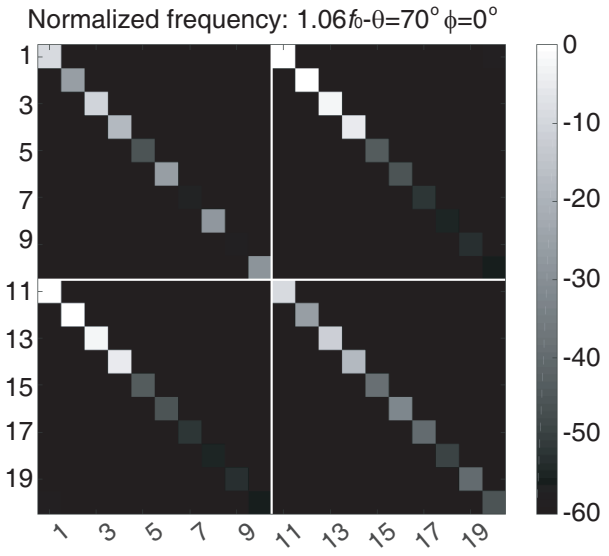

Index	Side	Fl. Mode	Index	Side	Fl. Mode
1	Input	TE_{00}	11	Output	TE_{00}
2	Input	TM_{00}	12	Output	TM_{00}
3	Input	TE_{-1-1}	13	Output	TE_{-1-1}
4	Input	TM_{-1-1}	14	Output	TM_{-1-1}
5	Input	TE_{11}	15	Output	TE_{11}
6	Input	TM_{11}	16	Output	TM_{11}
7	Input	TE_{0-1}	17	Output	TE_{0-1}
8	Input	TM_{0-1}	18	Output	TM_{0-1}
9	Input	TE_{-1-2}	19	Output	TE_{-1-2}
10	Input	TM_{-1-2}	20	Output	TM_{-1-2}

Figure 6. Absolute values in dB of a limited set of the GSM coefficients for the diamagneto-dielectric WAIM layers reported in Figure 4, obtained from full-wave simulations. I(nput)/O(utput) refer to the side of the layers cascade that is close/far to the phased array. Elements in the matrix refer to a set of 10 Floquet modes at the Input or Output side, as described by the table on bottom. The higher order modes coefficients are almost negligible and for this reason they are not shown here.

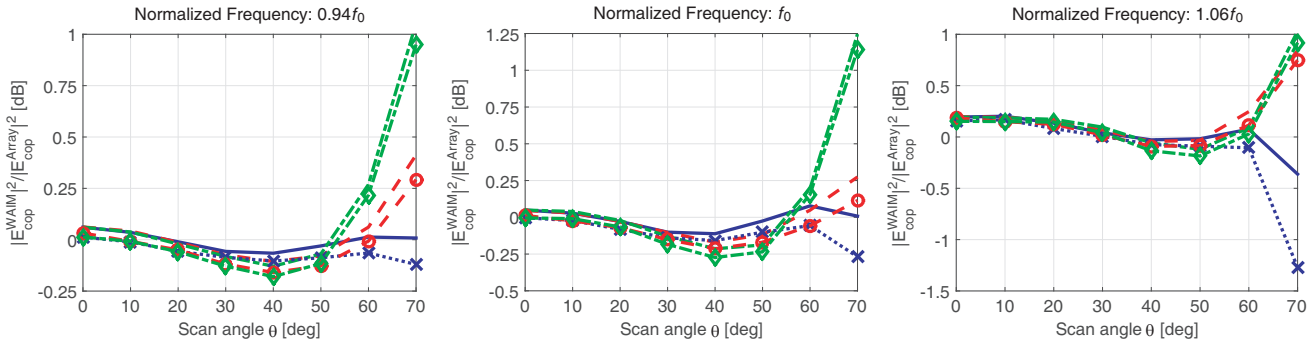

Figure 7. The same as Figure 5, but with line without markers referring to the semi-analytical results (solid blue lines: E-plane; dashed red lines: D-plane; dot-dashed green lines: H-plane) and line with markers referring to full-wave numerical results (dotted blue with cross lines: E-plane; dashed with circle red lines: D-plane; dot-dashed with diamond green lines: H-plane).

4. CONCLUSION

Since the seminal works on MMs have been published, they have shown a lot of potential applications, especially as means to improve the performances of EM devices beyond the classical or state-of-the-art limitations. The possibility of increasing the angular coverage ranges of phased arrays is one of these potential applications. In this work, we have presented an optimization procedure that allows to find the optimal values of volumetric anisotropic WAIM layers. Two different implementations of anisotropic MM-WAIM layers have been presented. The main innovations contained in this paper are:

- with respect to [7, 8, 13]: extension of the WAIM design strategy procedure to any possible active phased array (and not only canonical cases) by exploiting GSMs, computed by means of numerical full-wave softwares and analytical transmission line models;
- with respect to [7, 8, 9]: introduction of an improved cost function with adaptive weights;
- with respect to [7, 9, 13]: substantial improvements of the active phased array scanning performances at least on two planes, while keeping them almost unaltered on the third plane (fractional bandwidth 13%);
- with respect to all the previous works mentioned:
  - study of the influence of the anisotropic WAIM on the radiated copolar components. This allows monitoring the actual transmitted power and the effect of the WAIM layers on the copolar radiation component. This is an important parameter to be considered in realistic radar or satellite communication scenarios.
  - definition of a physical structure characterized by a diamagnetic-dielectric behavior, necessary to modify the active impedance for both polarizations and therefore the scanning characteristics of the array for all azimuthal planes.

ACKNOWLEDGMENT

The manuscript has been prepared in the framework of D-RACE (Dutch RAdar Centre of Expertise, a strategic alliance of Thales Nederland B.V. and TNO). The authors would like to thank Dr. Ir. Simon van den Berg, from Thales Nederland B.V., for the very fruitful discussions during the execution of the project. They further acknowledge Ir. Roland Bolt and Pierluigi Chiusolo, from TNO, for their support for numerical simulations.

REFERENCES

1. Magill, E. G. and H. A. Wheeler, "Wide-angle impedance matching of a planar array antenna by a dielectric sheet," *IEEE Transactions on Antennas and Propagation*, Vol. 14, No. 1, January 1966.
2. Hannan, P. W., D. Lerner, and G. Knittel, "Impedance matching a phased-array antenna over wide scan angles by connecting circuits," *IEEE Transactions on Antennas and Propagation*, Vol. 13, No. 1, January 1965.
3. Hansen, R. C., *Phased Array Antennas*, 2nd edition, John Wiley & Sons, Inc., Hoboken, New Jersey, 2009.
4. Pendry, J., A. Holden, W. Stewart, and I. Youngs, "Extremely low frequency plasmons in metallic mesostructures," *Physical Review Letters*, Vol. 76, No. 25, June 1996.
5. Pendry, J. B., A. J. Holden, D. J. Robbins, and W. J. Stewart, "Magnetism from conductors and enhanced nonlinear phenomena," *IEEE Transactions on Microwave Theory and Techniques*, Vol. 47, No. 11, 2075–2084, November 1999.
6. Smith, D. R., J. B. Pendry, and M. C. K. Wiltshire, "Metamaterials and negative refractive index," *Science*, Vol. 305, August 2004.
7. Sajuyigbe, S., M. Ross, P. Geren, S. A. Cummer, M. H. Tanielian, and D. R. Smith, "Wide angle impedance matching metamaterials for waveguide-fed phased-array antennas," *IET Microwaves, Antennas & Propagation*, Vol. 4, No. 8, 1063–1072, August 2010.

8. Oliveri, G., F. Viani, N. Anselmi, and A. Massa, "Synthesis of multilayer WAIM coatings for planar-phased arrays within the system-by-design framework," *IEEE Transactions on Antennas and Propagation*, Vol. 63, No. 6, 2482–2496, June 2015.
9. Rodriguez-Ulibarri, P., M. Beruete, F. Falcone, T. Crepin, C. Martel, F. Boust, C. Loecker, K. Herbertz, C. Salzburg, T. Bertuch, J. P. Martinaud, T. Dousset, and J. A. Marcotegui, "Metaradome for blind spot mitigation in phased-array antennas," *2014 8th European Conference on Antennas and Propagation (EuCAP)*, 2504–2508, April 6–11, 2014.
10. Silvestri, F., P. Chiusolo, L. Cifola, R. Bolt, G. Gerini, "Design of metamaterial based wide angle impedance matching layers for active phased arrays," *2015 9th European Conference on Antennas and Propagation (EuCAP)*, 1–5, April 13–17, 2015.
11. Felsen, L. B. and N. Marcuvitz, *Radiation and Scattering of waves*, IEEE Press, 1994.
12. Borgiotti, G. V., "A novel expression for the mutual admittance of planar radiating elements," *IEEE Transactions on Antennas and Propagation*, Vol. 16, No. 3, 329–333, May 1968.
13. Cameron, T. and G. Eleftheriades, "Analysis and characterization of a wide-angle impedance matching metasurface for dipole phased arrays," *IEEE Transactions on Antennas and Propagation*, accepted for publication.
14. Hansen, R. C., *Microwave Scanning Antennas*, Academic Press, 1966.
15. ANSYS® Electromagnetics Suite 15.0.0, ANSYS ® HFSS 2014, © 2013 SAP IP, Inc.
16. Ludwig, A. C., "The definition of cross polarization," *IEEE Transactions on Antennas and Propagation*, Vol. 21, 116–119, January 1973.
17. Bhattacharyya, A. K., *Phased Array Antennas*, John Wiley & Sons, Inc., Hoboken, NJ, 2006.
18. Haupt, R. L. and D. H. Werner, *Genetic Algorithms in Electromagnetics*, Wiley IEEE Press, 2007.
19. Matlab© R2011b, The Mathworks Inc.
20. Martini, E., G. M. Sardi, and S. Maci, "Homogenization processes and retrieval of equivalent constitutive parameters for multisurface-metamaterials," *IEEE Transactions on Antennas and Propagation*, Vol. 62, No. 4, 2081–2092, April 2014.
21. Chen, X., T. Grzegorczyk, B. I. Wu, J. Pacheco, and J. Kong, "Robust method to retrieve the constitutive effective parameters of metamaterials," *Physical Review E*, Vol. 70, Issue 1, July 2007.
22. Jiang, Z. H., J. A. Bossard, X. Wang, and D. H. Werner, "Synthesizing metamaterials with angularly independent effective medium properties based on an anisotropic parameter retrieval technique coupled with a genetic algorithm," *Journal of Applied Physics*, Vol. 109, 013515, January 2011.
23. Tretyakov, S., *Analytical Modeling in Applied Electromagnetics*, Artech House, Inc., Norwood, 2003.
24. Collin, R. E., "A simple artificial anisotropic dielectric medium," *IRE Transactions on Microwave Theory and Techniques*, Vol. 6, No. 2, 206–209, April 1958.
25. Collin, R. E., *Field Theory of Guided Waves*, 2nd edition, IEEE Press, Piscataway, NJ, 1991.